Int. J. Heat Mass Transfer Vol 28, No. 4, pp. 731–740, 1985
Printed in Great Britain

0017 9310/85 $3.00 + 0.00

Heat transfer and pressure drop in flow passages that are open along their lateral edges

E. M. SPARROW, P. C. STRYKER and C. A. C. ALTEMANI
Department of Mechanical Engineering, University of Minnesota, Minneapolis, MN 55455, U.S.A.

(*Received* 8 *August* 1984 *and in final form* 11 *October* 1984)

Abstract—Passage-average and local heat transfer coefficients and overall pressure drops were measured for both laminar and turbulent flow in a rectangular passage open along its lateral edges and closed at its downstream end. Parametric variations were made of the Reynolds number, the interwall spacing, and the passage configuration. For the latter, the inlet and exit fluid flow areas were: (1) both fully open, (2) half blocked at inlet, open at exit, and (3) half blocked at exit, open at inlet. The objective of the shrouding (i.e. the partial blockages) was to encourage the flow to penetrate into the downstream portion of the passage and, thereby, to promote the streamwise uniformity of the local transfer coefficient. For the unshrouded passage, the passage-average heat transfer coefficient increased by about 40% in response to a halving of the interwall spacing. The Reynolds number dependence of the transfer coefficient obeyed two distinct power laws, respectively for the high and low Reynolds number ranges. Partial shrouding of the inlet increased the passage-average transfer coefficient by 25–40% at the higher Reynolds numbers, while side shrouding yielded 10–15% enhancement at the lower Reynolds numbers. Streamwise uniformity of the local transfer coefficient was promoted by shrouding and by increases in the interwall spacing and the Reynolds number. The overall pressure drop increased in the presence of shrouding.

INTRODUCTION

SYSTEM-RELATED geometric constraints as well as potential gains in design and operating convenience may serve to motivate consideration of novel flow passage configurations for forced convection heating or cooling. The flow passages to be investigated here were so motivated, having originally been designed for air cooling of electronic equipment. Although these passages have the general form of a flat rectangular duct, they are distinctively unconventional in that the usual exit cross section is blocked, while the two lateral edges are open and serve as exits for the airflow. The heat transfer and pressure drop characteristics of such flow passages have not heretofore been dealt with in the published literature, and their determination is the focus of the present research, which is experimental in nature.

Figure 1 has been prepared to illustrate the type of flow passage being considered. The (a) part of the figure depicts the downstream wall of a plenum chamber in which there is an opening through which air passes into an array of parallel-plate channels (i.e. high-aspect-ratio rectangular ducts). To better display the nature of these flow passages, the plenum wall has been stripped away in Fig. 1(b). As seen there, the passages are the spaces between plate-type fins affixed to a baseplate from which heat is to be removed by the joint action of the fins and the airflow. (In the electronic cooling application, the baseplate is termed a heat sink.) The presence of the baseplate blocks the flow at the downstream end of the passage, forcing it to exit along the lateral edges of the fins, which are open.

The fluid flow and thermal events in all of the passages are the same, so that the heat transfer and pressure loss coefficients for any one passage are applicable to all. Also, the successful accomplishment of the research is substantially aided by the use of a single flow passage rather than an array of passages. In view of this, a single-passage model, as depicted schematically in Fig. 1(c), was employed in the present experiments. Note, however, that the solid surface which frames the flow passage inlet in Fig. 1(c) is wider than the solid surface which frames the individual flow passage inlets in Fig. 1(a). The effect of this difference in inlet geometry on the average heat transfer coefficient for the passage as a whole is expected to be small. This is because the streamwise lengths of the investigated passages were very much greater than the interwall spacing (by 42 to 82 times).

With a view toward providing information for various alternative flow passage geometries, experi-

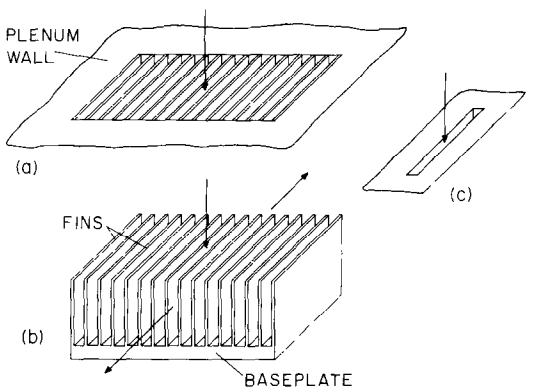

FIG. 1. Pictorial views of flow passages open along their lateral edges.

NOMENCLATURE

A_w area of mass transfer surfaces
$\mathscr{D}$ mass diffusion coefficient
K local mass transfer coefficient
$\bar{K}$ passage-average mass transfer coefficient, equation (1)
L side dimension of square wall of passage
ΔM change of mass of bounding walls
Δp overall pressure drop
Re rectangular-duct Reynolds number, $4\dot{w}/\mu[2(S+L)]$
S interwall spacing
Sc Schmidt number, $\nu/\mathscr{D}$
$\overline{Sh}$ passage-average Sherwood number, $\bar{K}L/\mathscr{D}$
V velocity at passage inlet, $\dot{w}/\rho(LS)$
$\dot{w}$ flowrate of air
x, y surface coordinates.

Greek symbols
δ surface recession
$\bar{\delta}$ mean recession
μ viscosity
ν kinematic viscosity
ρ density
$\rho_{n,w}$ naphthalene vapor density at passage wall
$\rho_{n,in}$ naphthalene vapor density at passage inlet
τ duration of data run.

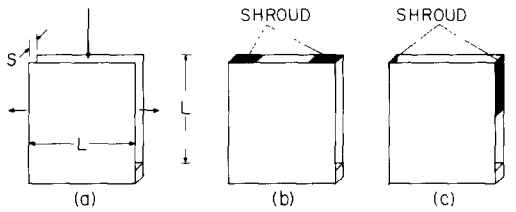

FIG. 2. Flow passage configurations.

ments were performed for the three configurations pictured in Figs. 2(a)–(c). The basic case is that of Fig. 2(a), where both the inlet and the lateral edges are fully open. In Fig. 2(b), the inlet is symmetrically shrouded such that the remaining opening area is half of the original opening area. In the third configuration, Fig. 2(c), the upper half of the lateral-edge outflow area is shrouded (on both sides). The shrouding arrangements pictured in Figs. 2(b) and 2(c) were intended to force the flow to penetrate farther into the passage before exiting at the lateral edges.

Figure 2(a) illustrates the dimensional nomenclature used to describe the flow passage geometry. As seen there, the passages considered here have square walls, i.e. equal length and width L, and the interwall spacing is S. Experiments were performed for four values of the S/L ratio equal to 0.012, 0.015, 0.019 and 0.024.

Three parameters were varied during the course of the experiments. One of these is the passage configuration, as defined by Figs. 2(a)–(c), while the second is the S/L ratio. For each flow passage geometry specified by these two parameters, the Reynolds number Re (defined as for a conventional rectangular duct) was varied from about 600 to 9000.

The main quantities for which results were obtained include the average heat transfer coefficient for the passage as a whole and the overall pressure drop. These quantities are presented in dimensionless form and are, therefore, independent of the specific dimensions of the apparatus, but depend on the parameters S/L, Re and the passage configuration, Figs. 2(a)–(c). Semi-quantitative results were also obtained for the distribution of the local heat transfer coefficient along the bounding walls of the flow passage. The heat transfer results correspond to the isothermal-wall boundary condition which, in the case of fins, implies a fin efficiency equal to one.

EXPERIMENTAL

In order both to simplify the apparatus and to enhance the accuracy of the results, the experiments were performed by means of the naphthalene sublimation technique in lieu of direct heat transfer measurements. Correspondingly, the surfaces which bounded the flow passage were of solid naphthalene. The amount of mass sublimed from these surfaces during a data run was measured and, from this, the average mass transfer coefficient for the passage as a whole was evaluated. Measurements were also made of the mass that was locally sublimed as a function of position on the bounding surfaces, yielding local mass transfer coefficients.

These mass transfer results can be transformed to heat transfer results by employing the well-established analogy between heat and mass transfer. The boundary conditions for the mass transfer (uniform concentration of the naphthalene vapor) transforms to uniform wall temperature for the analogous heat transfer problem. Pressure drop measurements were made in a separate test setup in which there was no mass transfer.

Experimental apparatus

The flow passage used in the mass transfer experiments will be described with the aid of Fig. 3. The (a) part of the figure is a pictorial view of one of the passage walls, while the two-wall assembly is shown pictorially in the (b) part. In part (c), the installation of the flow passage assembly in the upper wall of a test chamber is illustrated.

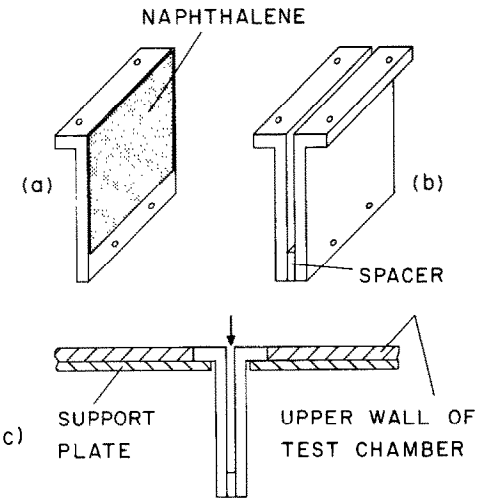

FIG. 3. Schematic diagrams of the experimental apparatus.

In essence, each wall [Fig. 3(a)] is an aluminum plate into which a cavity was machined to accommodate a layer of naphthalene that is implanted by a casting process. Furthermore, an integral, wing-like extension emanating from the upper rear of the plate was provided to facilitate the mating of the flow passage assembly with the test chamber. The plate proper is 0.635 cm thick, and the naphthalene cavity occupies about half the plate thickness. The exposed face of the naphthalene, a 10.16 cm square, is framed by the metallic walls of the cavity. The frame thickness is 0.0317 cm at the side edges and 0.0635 cm at the top. At the bottom, the broad frame serves as a bearing surface for a spacer which is used to fix the separation distance between the two walls of the flow passage. The indicated screw holes in the bottom-edge frame are used when the spacer is secured, while the holes in the extension piece accommodate screws which anchor the passage wall to the test chamber.

The assembled flow passage [Fig. 3(b)] includes the two principal walls plus the aforementioned spacer. As seen in the figure, the spacer also serves as a closure at the downstream end of the flow passage. Each spacer was made of brass and was hand-sanded and polished to the desired thickness. The four spacers employed during the course of the experiments had thicknesses of 0.124, 0.152, 0.191 and 0.241 cm, respectively.

During a data run, the assembled flow passage was situated in a specially designed seat in the upper wall of a large test chamber [Fig. 3(c)]. The wing-like extensions of the passage assembly rested on and were fastened to a pair of support plates, as shown in the figure. The separation distance between the support plates was made variable so as to accommodate the various flow-passage interwall spacings.

The shrouding of the inlet cross section of the flow passage, as illustrated in Fig. 2(b), was accomplished by the use of 0.0076-cm-thick, stainless steel shim stock. The shim strips were anchored to the upfacing surface of the passage assembly by double-sided tape. With these shrouds in place, the central half of the inlet cross section remained open. For the lateral-edge shrouding shown in Fig. 2(c), the upper half of the exit opening was sealed with 0.0020-cm-thick, pressure-sensitive polyester tape. The extreme thinness of the tape enabled it to be employed as a closure without necessitating machining of the apparatus.

The naphthalene surfaces which bound the flow passage were produced by a casting process. As a first step, the naphthalene remaining from the preceding data run was removed from the cavity in the flow passage wall by melting and evaporation. Then, the wall is placed face down on a flat, highly polished stainless steel plate, thereby forming a mold cavity. Molten naphthalene is poured into the cavity through an aperture in the rear face of the wall. After the solidification is completed, the mold parts are separated, exposing a solid naphthalene surface whose finish is equal to that of the polished plate against which it was cast.

In one of the walls, a thermocouple was embedded in the naphthalene during the casting process. The thermocouple junction was positioned flush with the exposed surface of the naphthalene. The temperature sensed by this thermocouple was employed to calculate the vapor pressure of the naphthalene at the bounding surface of the flow passage.

The test chamber is a large rectangular enclosure, 61×61 cm in horizontal cross section and 152.4 cm high. It is completely airtight except for the flow passage inlet situated in its upper wall and an exit port in its lower wall.

Experimental procedure

The system was operated in the suction mode, with air drawn from the laboratory into and through the flow passage. Upon leaving the passage, the air traversed the height of the test chamber, exited at the bottom, and passed along a pipeline to a flowmeter (a calibrated orifice), a control valve, and a blower. The blower was situated in a service corridor adjacent to the laboratory, and its compression-heated, naphthalene-laden discharge was vented outside the building.

In the primary set of mass transfer experiments, the focus of each data run was to determine the change of mass of each passage wall during a measured period of time. Mass measurements were made before and after the run with a Sartorius ultra-precision balance with a resolution of 10^{-5} g and a capacity of 166 g. The duration of the run was selected so that the spatial-mean recession of the naphthalene surface of each wall was limited to 0.0013 cm. Following the actual data run, a calibration run was made to determine the extraneous mass losses during the setup and disassembly of the apparatus, yielding a correction of about 1%.

In supplementary mass transfer experiments, the contours of the naphthalene surfaces were measured both before and after each run. These measurements were made with a stylus-type instrument which sensed

the elevation of the stylus tip electronically. The nominal resolving power of the instrumentation was 0.000025 cm.

For the data runs in which pressure drop information was collected, the naphthalene surfaces bounding the flow passage were replaced by surfaces of solid benzoic acid. The benzoic acid was cast in place by a procedure identical to that used for the casting of the naphthalene. The use of benzoic acid was motivated by its relatively low vapor pressure (compared with naphthalene), so that virtually no sublimation occurred during a pressure drop run.

The pressure drop was measured with the aid of a pressure tap installed in the wall of the test chamber (there were two such taps which always read the same). Signals from this tap were conveyed to one port of a capacitance-type, solid-state pressure meter, while the other port of the meter was open to the ambient. The resulting difference yielded the flow-passage pressure drop, including the naturally occurring inlet and exit losses.

DATA REDUCTION

The average mass transfer coefficient $\bar{K}$ for the flow passage as a whole was evaluated from the defining equation

$$\bar{K} = \frac{\Delta M/\tau A_w}{\rho_{n,w} - \rho_{n,in}}. \quad (1)$$

In this equation, ΔM is the change of mass of the two principal walls of the flow passage during the duration τ of the data run, and A_w is the area of the naphthalene bounding surfaces. The denominator is the difference between the naphthalene vapor densities at the bounding surfaces and at the passage inlet, $\rho_{n,w}$ and $\rho_{n,in}$, respectively. The latter is zero in the present experimental setup. To evaluate the former, the vapor pressure—temperature relation for naphthalene was used in conjunction with the perfect gas law, with the measured surface temperature as input. Note that the heat transfer coefficient $\bar{h}$ corresponding to the $\bar{K}$ of equation (1) is given by $\bar{h} = (Q/A_w)/(T_w - T_{in})$, in which Q is the rate of heat transfer at the bounding walls, and T_w and T_{in} are the wall and inlet temperatures, respectively.

A dimensionless representation of the $\bar{K}$ values is provided by the Sherwood number $\overline{Sh}$ (the mass transfer counterpart of the Nusselt number). For the selection of the characteristic dimension in the Sherwood number, two approaches were considered. One approach is to employ a quantity such as the hydraulic diameter which varies with the interwall spacing S, the motivation being to try to eliminate S as a separate parameter. In the initial processing of the data, the hydraulic diameter was used in the Sherwood number, but the effect of S was not wholly eliminated. The second approach is to employ a characteristic dimension in $\overline{Sh}$ which was constant throughout the course of the experiments, so that variations of $\overline{Sh}$ are true reflections of variations of $\bar{K}$ (and only of $\bar{K}$).

The latter approach was adopted here. Since the present results are intended to be applied to passages having walls with surface dimensions L by L, and since L was constant throughout the experiments, $\overline{Sh}$ was defined as

$$\overline{Sh} = \bar{K}L/\mathscr{D}. \quad (2)$$

The diffusion coefficient $\mathscr{D}$ appearing in equation (2) was eliminated by employing the definition of the Schmidt number ($Sc = \nu/\mathscr{D}$), so that

$$\overline{Sh} = (\bar{K}L/\nu)Sc \quad (3)$$

where $Sc = 2.5$ for naphthalene diffusion in air.

The surface distribution of the local mass transfer coefficient K will be presented via the ratio $K/\bar{K}$. In this regard, let $\delta(x, y)$ denote the surface recession at a location (x, y) during a data run, and let

$$\bar{\delta} = \int_{A_w} \delta(x, y)\, dA_w/A_w \quad (4)$$

so that

$$K/\bar{K} = \delta/\bar{\delta}. \quad (5)$$

The measured flow-passage pressure drop Δp was made dimensionless by the velocity head $\frac{1}{2}\rho V^2$. The velocity V was evaluated at the inlet of the passage

$$V = \dot{w}/\rho(LS) \quad (6)$$

in which $\dot{w}$ is the mass flowrate of the air. Note that the area LS of the unshrouded inlet was employed in the evaluation of V for all of the passage configurations, even that in which the inlet was partially shrouded. Thus, for given values of the interwall spacing S and mass flow $\dot{w}$, $\frac{1}{2}\rho V^2$ is the same for both the unshrouded and shrouded configurations. This approach was adopted so that $\Delta p/(\frac{1}{2}\rho V^2)$ would be a true reflection of Δp when different shrouding arrangements were used for a passage with a fixed interwall spacing.

The mass transfer and pressure drop results will be parameterized by the Reynolds number Re, which was defined as for a conventional rectangular duct having cross-sectional dimensions S by L

$$Re = 4\dot{w}/\mu[2(S+L)] \quad (7)$$

where $2(S+L)$ is the perimeter of the rectangular duct. It is relevant to note that $(S+L)$ varied by only 1% over the investigated range of interwall spacings. Therefore, for all practical purposes, the Reynolds number can be regarded as a dimensionless mass flow.

RESULTS AND DISCUSSION

Passage-average mass transfer coefficient

In the basic configuration, both the inlet and the lateral-edge flow areas are fully open, as pictured in Fig. 2(a). The passage-average Sherwood numbers for this configuration are presented in Fig. 4 as a function of the Reynolds number over the range from about 600 to

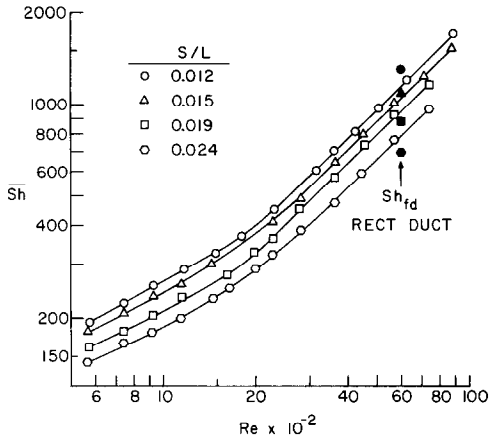

FIG. 4. Passage-average Sherwood numbers for the unshrouded flow passage.

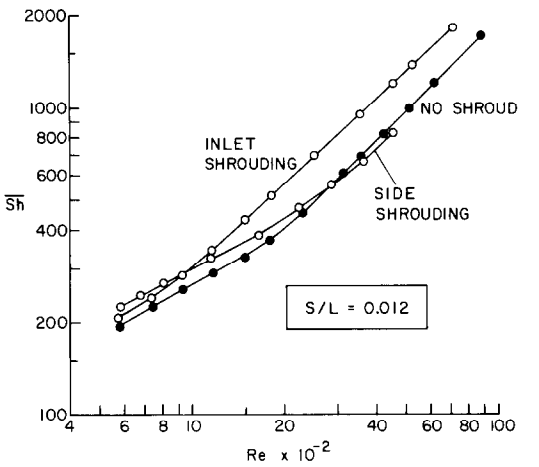

FIG. 5. Effect of partial shrouding of the inlet or side fluid flow areas on the passage-average Sherwood number, $S/L = 0.012$.

9000. The figure conveys data for the four investigated interwall spacings, which are characterized by the S/L ratio which ranges from 0.012 to 0.024. Curves have been faired through the data for each fixed S/L to provide continuity. In appraising the results, it is relevant to recall that the Sherwood number is a direct reflection of the mass transfer coefficient (i.e. the characteristic dimension in $\overline{Sh}$ is common to all the investigated cases).

The figure shows that the passage-average mass transfer coefficient increases as the interwall spacing decreases. At a fixed Reynolds number, the increase in the coefficient is about 40% as S/L varies from 0.024 to 0.012. Since a fixed Reynolds number implies a fixed mass flowrate, a decrease in the interwall spacing results in an increase of the velocities in the passage, bringing about an increase in the transfer coefficient.

As expected, the mass transfer coefficient increases with increasing Reynolds number. At the higher Reynolds numbers, $Re > \sim 3000$, the $\overline{Sh}$, Re curves for the various interwall spacings are parallel straight lines, signaling a commonality of flow regime. In this Reynolds number range, $\overline{Sh} \sim Re$. At Reynolds numbers below about 3000, the $\overline{Sh}$, Re distributions deviate from the aforementioned straight lines, suggesting a change of flow regime. For $Re < \sim 1500$, the distributions are approximately represented by $\overline{Sh} \sim Re^{1/2}$. The change of flow regime which appears to occur between $Re = 1500$ and 3000 is, in all likelihood, a laminar–turbulent transition.

The uniqueness of the investigated passage geometry precludes definitive comparisons of the results of Fig. 4 with the literature. A qualitative comparison can, however, be made with mass transfer coefficients from [1] for a conventional flat rectangular duct. The only Reynolds number of [1] that falls in the present range is $Re = 6000$, and the corresponding fully developed mass transfer coefficient, rephrased in terms of the present Sherwood number definition, is shown by the black symbols in Fig. 4. The level of agreement between these rectangular duct Sherwood numbers and those for the present flow passage is surprisingly good, despite the fact that the former are fully developed values and the latter are passage-average values.

Attention is now turned to the response of the passage-average Sherwood number to partial shrouding of the fluid inlet or the fluid exit. The Sherwood number results for the investigated shrouding configurations are compared with those for the unshrouded passage in Figs. 5–8, where each figure corresponds to a fixed interwall spacing S/L. In each figure, the Sherwood number results for the unshrouded passage are depicted by black symbols in order to emphasize their role as a baseline. The data labeled *inlet shrouding* correspond to configuration (b) of Fig. 2, while those labeled *side shrouding* are for configuration (c).

An overall examination of Figs. 5–8 reveals that the effects of shrouding on the passage-average Sherwood number are qualitatively similar at all the interwall spacings. Compared with the baseline (no shrouding)

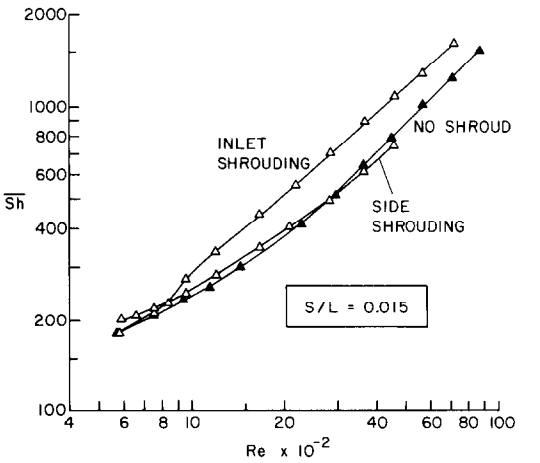

FIG. 6. Effect of partial shrouding of the inlet or side fluid flow areas on the passage-average Sherwood number, $S/L = 0.015$.

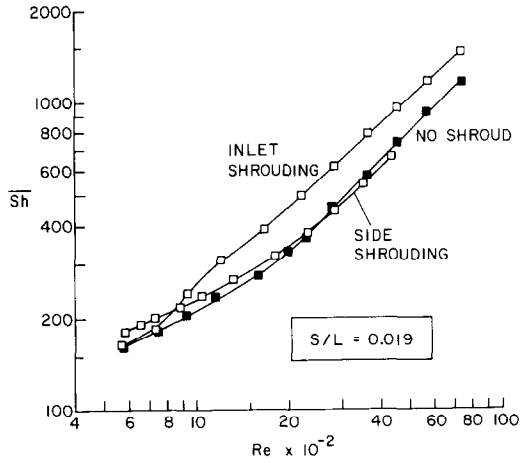

FIG. 7. Effect of partial shrouding of the inlet or side fluid flow areas on the passage-average Sherwood number, $S/L = 0.019$.

case, the partial shrouding of the passage inlet is enhancing over the entire investigated Reynolds number range. The extent of the enhancement is of the order of 25–40% for $Re > \sim 1500$ and is relatively uniform in that range. This increase in the Sherwood number, while significant, must be viewed in terms of the associated pressure drop penalty, which will be presented shortly.

As the Reynolds number decreases, the Sherwood numbers for the inlet-shrouded passage tend to dip downward and approach those for the baseline case. At the low end of the Reynolds number range, there is virtually no enhancement due to inlet shrouding. This downward dipping is believed due to a change in the structure of the eddies which are situated behind the shrouds.

Partial shrouding of the sides of the passage yields an altogether different response from that described in the foregoing paragraphs. As seen in Figs. 5–8, side shrouding actually reduces the Sherwood numbers for $Re > 2500$–3000, for three of the four interwall spacings, while for the fourth spacing the Sherwood number results for the shrouded and unshrouded cases are virtually identical. With decreasing Reynolds number, the side-shrouded Sherwood numbers tend to drift above the no-shroud values, so that at the very low end of the range there is enhancement at the 10–15% level. Thus, from the standpoint of heat transfer enhancement, side shrouding does not appear to be very effective.

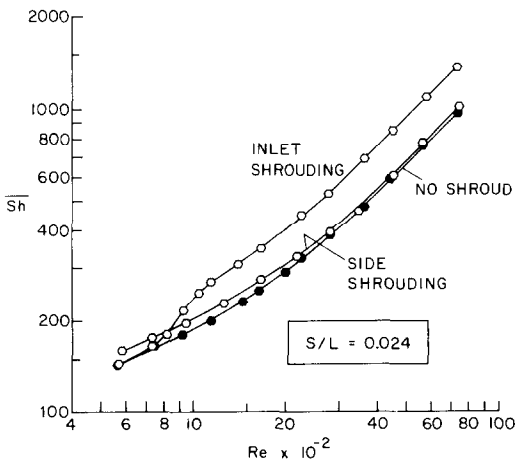

FIG. 8. Effect of partial shrouding of the inlet or side fluid flow areas on the passage-average Sherwood number, $S/L = 0.024$.

Overall pressure drop

The dimensionless pressure drop results for all of the investigated passage configurations and interwall spacings are presented in Fig. 9. On the ordinate, the overall pressure drop Δp (which includes inlet and exit losses in addition to losses internal to the passage) is made dimensionless by the velocity head $\frac{1}{2}\rho V^2$. Note that V is defined so that its value for a given interwall spacing is the same regardless of the presence or absence of shrouding. Thus, at a given Reynolds number (i.e. a given mass flowrate) and a fixed interwall spacing, shrouding-related changes in $\Delta p/\frac{1}{2}\rho V^2$ are true reflections of the changes in Δp.

The most striking feature of Fig. 9 is the stratification of the data as a function of the shrouding configuration. As expected, the lowest pressure drop among the investigated configurations is that for the no-shroud case. Side shrouding increases the pressure drop by about 70%, while inlet shrouding gives rise to a pressure drop increase of about 150%. The qualitative ordering of these results is physically reasonable.

Within each band of data corresponding to a particular shrouding configuration, there is only a modest spread with S/L, indicating that the effect of interwall spacing on Δp is satisfactorily correlated by the selected normalization. In addition, $\Delta p/\frac{1}{2}\rho V^2$ tends to level off at higher Reynolds numbers. This is a characteristic common to flows where inertial losses play a significant role.

It is relevant to compare the pressure drop results of Fig. 9 with those for a conventional flat rectangular duct. Data for the latter are available in [1] for $Re = 6000$. By the use of Fig. 10 of [1], $\Delta p/\frac{1}{2}\rho V^2$

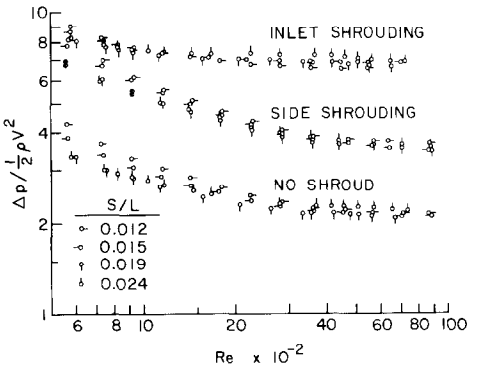

FIG. 9. Overall pressure drop results.

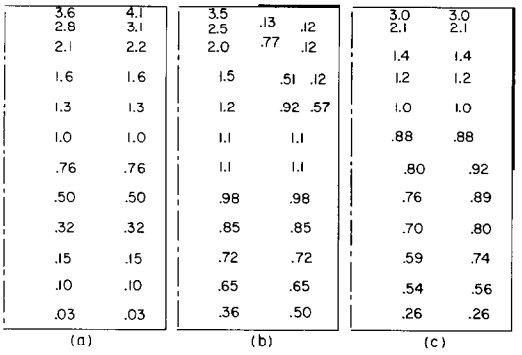

FIG. 10. Dimensionless distributions of the local mass transfer coefficient $K/\bar{K}$ for $Re \simeq 600$ and $S/L = 0.012$.

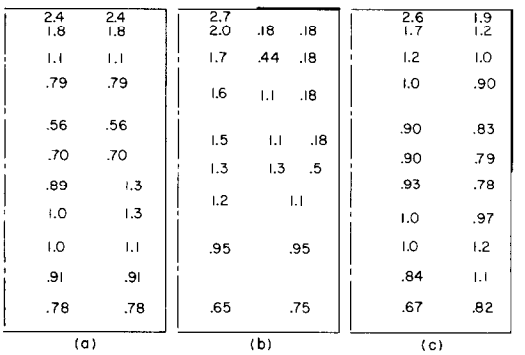

FIG. 12. Dimensionless distributions of the local mass transfer coefficient $K/\bar{K}$ for $Re \simeq 4500$ and $S/L = 0.012$.

was calculated to be 2.70 and 2.04, respectively for rectangular ducts with cross sections $S/L = 0.012$ and 0.024 and streamwise length equal to that of the present flow passage. These calculated values include both the inlet losses and the internal losses in the duct but not the exit losses.

The aforementioned numerical values of $\Delta p/\frac{1}{2}\rho V^2$ for the rectangular duct are comparable in magnitude to those of Fig. 9 for the no-shroud case at $Re = 6000$ (which also include exit losses). At low Reynolds numbers (e.g. 600), a comparison based on the laminar friction factor ($f = 96/Re$) for a parallel-plate channel indicates that the present no-shroud pressure drop is lower than that of the channel.

Local transfer coefficients

Distributions of the local mass transfer coefficient were measured for a total of 12 cases. These cases include the smallest and largest interwall spacings, $S/L = 0.012$ and 0.024, and two Reynolds numbers, $Re \simeq 600$ and 4500, which respectively correspond to the low and high ends of the investigated range. For each of the four S/L, Re combinations, local coefficients were determined for all three flow passage configurations [Figs. 2(a)–(c)].

The local mass transfer rates were deduced by differencing surface contour measurements made before and after a data run. The changes in the surface contour were kept small (by proper selection of the duration of the run) so as not to significantly alter the flow passage geometry, the mean recession of the surface being about 0.0013 cm. Since recessions of this small magnitude were determined by the aforementioned differencing of two sets of contour measurements, it was essential that the position of the naphthalene surface with respect to the contour measuring instrument be identical for each set of measurements. Extreme care was taken with the positioning of the surface during the measurements, but residual uncertainties in the contours of the order of 0.00005–0.00013 cm may well have existed. In view of this, the local mass transfer coefficients are regarded as semi-quantitative.

The distributions of the local mass transfer coefficient K are presented in Figs. 10–13 in terms of the ratio $K/\bar{K}$, where $\bar{K}$ is the average coefficient. Each of the successive figures corresponds to a specific (Re, S/L) combination, namely, (600, 0.012), (600, 0.024), (4500, 0.012), and (4500, 0.024). Each figure consists of (a), (b), and (c) parts, which respectively convey results for the no-shroud case, the inlet-shrouded case, and the side-shrouded case. Each part is a layout of the passage wall, bounded at the left by the streamwise symmetry line. The flow enters at the top and exits along the right-hand

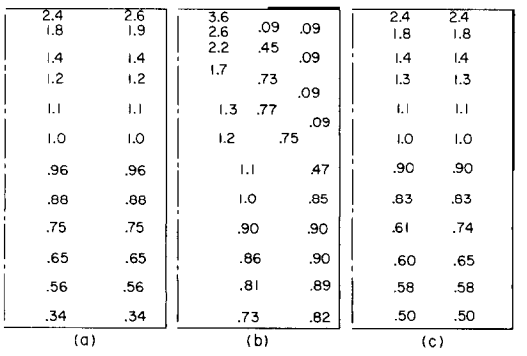

FIG. 11. Dimensionless distributions of the local mass transfer coefficient $K/\bar{K}$ for $Re \simeq 600$ and $S/L = 0.024$.

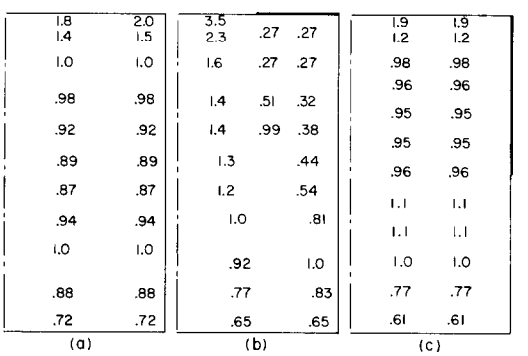

FIG. 13. Dimensionless distributions of the local mass transfer coefficient $K/\bar{K}$ for $Re \simeq 4500$ and $S/L = 0.024$.

side. In the (b) and (c) parts, the shrouding is depicted by the heavy lines.

The numbers appearing in the layouts are values of $K/\bar{K}$. Each number pertains to the general neighborhood of the site where it is marked.

An overall inspection of Figs. 10–13 reveals certain common features. For all cases, the transfer coefficient attains its highest value at the inlet and decreases in the direction from the inlet to the blocked downstream end of the flow passage. The extent of this streamwise decrease depends on the specifics of each case, but it is significant in all cases. Thus, if the passage walls are fins attached to a base surface, the highest transfer coefficients occur at the fin tip and the lowest occur at the base. In contrast to the large streamwise variations, the transverse variations of the transfer coefficient are moderate, except when they are forced by the presence of the inlet shroud.

Specific attention will first be turned to the results for the smallest interwall spacing and lowest Reynolds number (Fig. 10). For the no-shroud case (part (a) of the figure), the streamwise variations in the transfer coefficient are the largest among all the investigated cases. These variations result from the inability of the low Reynolds number flow to penetrate to the downstream end of the passage in the face of the large hydrodynamic resistance created by the narrow interwall spacing. The flow, in attempting to find the path of least resistance, seeks an early exit along the lateral edges of the flow passage.

With the side shroud in place, the aforementioned early exiting of the flow from the passage is blocked. As a consequence, as shown in Fig. 10(c), the streamwise variation of the transfer coefficient is diminished relative to that of the no-shroud case [Fig. 10(a)]. However, the remaining streamwise variation is still appreciable.

The partial shrouding of the inlet increases the initial streamwise momentum of the flow and forces it away from the lateral edges in the upstream portion of the passage. Thus, the flow penetrates more deeply into the passage than in the no-shroud case, as witnessed by the diminished (but still considerable) streamwise variation of the transfer coefficient. However, the inlet shrouding sets up a pocket of relatively low velocity flow just downstream of the shroud, with resulting low values of the transfer coefficient.

The next figure, Fig. 11, pertains to the same low value of the Reynolds number as in Fig. 10, but now the interwall spacing is the largest among those investigated (rather than the smallest). The effect of the larger spacing is to decrease the hydrodynamic resistance and, as a consequence, the flow is more able to penetrate into the downstream region of the passage. This deeper penetration brings about an increase (relative to the average) of the downstream-region transfer coefficients. As a result, for each of the three passage configurations, the overall streamwise variation of the mass transfer coefficients in Fig. 11 is reduced relative to that of Fig. 10.

Figure 12 is the high Reynolds number counterpart of Fig. 10. The higher streamwise momentum of this flow is better able to overcome the hydrodynamic resistance of the narrow passage, with a consequent deeper penetration into the downstream region of the passage. Thus, the streamwise variations in evidence in Fig. 12 are substantially smaller than those of Fig. 10.

In Fig. 13, results are presented for the largest of the spacings and Reynolds numbers for which local measurements were made, that is, an increase in Re relative to Fig. 11 and an increase in S/L relative to Fig. 12. The aforementioned trend toward greater streamwise uniformity of the transfer coefficient with increased Reynolds number is also in evidence for both the unshrouded and side-shrouded passages [compare Figs. 13(a, c) with Figs. 11(a, c)], but to a lesser extent than that evidenced by Figs. 10 and 12. For these passages, the trend with interwall spacing [Figs. 13(a, c) and 12(a, c)] is also maintained, albeit moderately. For the inlet-shrouded configuration, the changes between Figs. 11 and 13 and between Figs. 12 and 13, while moderate, do not conform to a clear trend.

The foregoing comparisons suggest that once either the Reynolds number or the interwall spacing is moderately large, increases in the other of the two parameters do not produce major changes in the extent of the streamwise variation of the transfer coefficient.

CONCLUDING REMARKS

The experimental work performed here has provided mass (heat) transfer and pressure drop data for a class of unconventional rectangular-duct type flow passages. The downstream end of the passage is closed, while the lateral edges are open and serve as exits for the airflow. Measurements were made both for the passage-average mass transfer coefficient and for the distribution of the local mass transfer coefficient on the bounding walls. Overall pressure drops, including the losses at the inlet, internal to the passage, and at the exit, were also measured.

These results were obtained for a range of the Reynolds number which encompassed both laminar and turbulent flow. Parametric variations were also made in the spacing between the passage walls and in the passage configuration. Three configurations were investigated. In one, the fluid inlet and exit areas were fully open. In the others, either the inlet or the exit areas were partially shrouded with the objective of encouraging the flow to penetrate into the downstream region of the passage and, by this, to make for greater streamwise uniformity of the local mass transfer coefficient. The shrouding covered half of the otherwise open area.

For the unshrouded flow passage, the passage-average transfer coefficient increased by about 40% in response to a halving of the interwall spacing. In the upper range of the Reynolds number, the transfer

coefficient increased more or less linearly with the Reynolds number, while in the lower range, the increase approximately followed a square-root relation. Partial shrouding of the inlet gave rise to a 25–40% increase of the passage-average transfer coefficient at higher Reynolds numbers but had little effect at lower Reynolds numbers. On the other hand, side shrouding was ineffectual at higher Reynolds numbers and provided a 10–15% enhancement at lower Reynolds numbers.

The overall pressure drop was strongly affected by the nature of the duct configuration, with the lowest pressure drop for the unshrouded passage and with increasingly larger pressure drops for the side-shrouded passage and for the inlet-shrouded passage. The effect of the interwall spacing on the pressure drop was well correlated in terms of the velocity head.

The measured local distributions of the mass transfer coefficient displayed substantial streamwise variations but only moderate transverse variations (except for localized transverse variations induced by inlet shrouding). Both inlet shrouding and side shrouding led to greater streamwise uniformity, as did increases in the interwall spacing and the Reynolds number.

REFERENCE

1. E. M. Sparrow and N. Cur, Maldistributed inlet flow effects on turbulent heat transfer and pressure drop in a flat rectangular duct, *J. Heat Transfer* **105,** 527–535 (1983).

TRANSFERT THERMIQUE ET PERTE DE CHARGE POUR DES ECOULEMENTS DANS DES PASSAGES DISTRIBUTEURS

Résumé—Des coefficients de transfert moyen et de perte de charge sont mesurés pour des écoulements laminaires et turbulents dans un passage rectangulaire ouvert sur les bords latéraux et fermé à l'extrémité en aval. On réalise une variation paramétrique du nombre de Reynolds, de l'espacement et de la configuration du passage. Pour cette dernière, les sections d'entrée et de sortie du fluide sont : (1) toutes les deux pleinement ouvertes ; (2) à moitié fermée à l'entrée, ouverte à la raison de l'épaulement (la fermeture partielle) est d'encourager le fluide à pénétrer dans la portion reculée du passage et par la suite de favoriser l'uniformité de l'écoulement et du coefficient de transfert local. Pour le passage sans épaulement, le coefficient de transfert moyen augmente d'environ quarante pour cent, en réduisant de moitié l'espacement. La dépendance du coefficient de transfert au nombre de Reynolds obéit à deux lois distinctes de puissance, respectivement pour les domaines de nombre de Reynolds élevés et bas. Une fermeture partielle de l'entrée augmente le coefficient de transfert moyen de 25–40 pour cent aux plus grands nombres de Reynolds, tandis qu'une fermeture latérale conduit à 10–15 pour cent d'augmentation aux faibles nombres de Reynolds. L'uniformité du coefficient de transfert local est favorisé par l'épaulement et par l'augmentation de l'intervalle d'espacement et du nombre de Reynolds. La perte de charge globale croît avec la présence de l'épaulement.

WÄRMEÜBERGANG UND DRUCKABFALL IN STRÖMUNGSKANÄLEN, DIE AN DEN SEITLICHEN ENDEN OFFEN SIND

Zusammenfassung—An einem rechtwinkligen Kanal, der an den seitlichen Enden offen und stromab geschlossen war, wurden der örtliche und der über den Kanal gemittelte Wärmeübergangskoeffizient sowie der Druckabfall bei laminarer und turbulenter Strömung gemessen. Parameter waren die Reynolds-Zahl, der Intervallabstand und die Kanalkonfiguration. Folgende Einlauf- und Auslaufbedingungen wurden untersucht: (1) Einlauf und Auslauf ganz offen; (2) halbgeschlossener Einlauf, offener Auslauf; (3) halbgeschlossener Auslauf, offener Einlauf. Durch die teilweise Schließung wurde die Strömung gezwungen, in den stromabwärts gelegenen Teil des Kanals einzudringen und dadurch für einen gleichmäßigen Wärmeübergang in Strömungsrichtung zu sorgen. Bei dem nichtgestörten Strömungskanal stieg der über den Kanal gemittelte Wärmeübergangskoeffizient um etwa 40% an, wenn man den Intervallabstand halbierte. Die Abhängigkeit des Wärmeübergangs von der Reynolds-Zahl folgt zwei bestimmten Potenzgesetzen für hohe bzw. niedrige Reynolds-Zahlen. Die teilweise Blockade des Einlaufs verbesserte den mittleren Wärmeübergangskoeffizienten um 25–40% bei höheren Reynolds-Zahlen, während die Blockade an den Seiten zu 10–15% Verbesserung bei niederen Reynolds-Zahlen führte. Die Gleichförmigkeit des örtlichen Wärmeübergangskoeffizienten wurde durch die Blockade und durch die Vergrößerung von Intervallabstand und Reynolds-Zahl verbessert. Der Gesamtdruckabfall stieg durch die Blockade an.

ТЕПЛООБМЕН И ПЕРЕПАД ДАВЛЕНИЯ В КАНАЛАХ С ПЕРФОРИРОВАННЫМИ БОКОВЫМИ ПОВЕРХНОСТЯМИ

Аннотация—Измерены перепады давления, локальные и осредненные по длине канала коэффициенты теплообмена для ламинарного и турбулентного режимов течения в прямоугольном канале с заглушенным торцом и перфорированными боковыми поверхностями. При измерениях варьировались числа Рейнольдса, расстояния между стенками и форма канала. Для прямоугольного канала рассматривались следующие случаи: (1) входное и выходные отверстия полностью открыты, (2) вход наполовину прикрыт, выход открыт, (3) выход наполовину прикрыт и открыт вход. Цель экранирования (т.е. частичного перекрытия)— способствовать проникновению потока в глубинные области канала (вниз по течению) и тем самым поддерживать постоянство коэффициента локального переноса по длине. Для неэкранированного канала средний коэффициент теплообмена увеличивается примерно на 40% при уменьшении вдвое расстояния между стенками. Зависимость коэффициента теплообмена от числа Рейнольдса подчиняется двум четким степенными законам, соответствующим диапазонам больших и малых чисел Рейнольдса. Частичное экранирование входа увеличивает средний коэффициент теплообмена на 25–40% при больших числах Рейнольдса, в то время как боковое экранирование приводит к 10–15%-ному увеличению при меньших числах Рейнольдса. Постоянство локального коэффициента теплообмена по длине поддерживалось экранированием и увеличением числа Рейнольдса и расстояния между стенками. При наличии экранирования увеличивался суммарный перепад давления.